General Analytical Model for Inductive Power Transfer System with EMF Canceling Coils

Keita Furukawa, Keisuke Kusaka, and Jun-ichi Itoh
Department of Electrical Engineering, Nagaoka University of Technology, NUT
Niigata, Japan

*E-mail: itoh@vos.nagaokaut.ac.jp, kusaka@vos.nagaokaut.ac.jp, archer_FK@stn.nagaokaut.ac.jp

***Abstract*- This paper provides an analytical model and design criteria of additional windings for reducing electromagnetic field (EMF) generated from inductive power transfer (IPT) systems. In particular, the canceling coils are connected to the main transmission coils with common-mode connection or differential-mode connection. Otherwise, the canceling coils are short-circuited. Parameter variation, which may degrade the system efficiency, occurs in the IPT system due to the unwanted coupling between the main transmission coils and the canceling coils. Therefore, theoretical analysis of the IPT system with the canceling coils is conducted in order to evaluate the effects of the EMF shielding methods on the system parameter variation. The calculation results of the system parameters agree to the measurement results in the prototype of the four-winding transformer with the error of lower than 5%.**

Keywords— active shielding, electromagnetic field, inductive power transfer, multiple magnetic coupling

I. INTRODUCTION

In recent years, inductive power transfer (IPT) systems have attracted much attention in terms of safety and convenient battery chargers for electrical vehicles (EVs) [1−5]. The IPT systems achieve power transmission using a magnetic coupling without electrical contacts. Electromagnetic field (EMF) should be considered because EMF may cause health impairment or malfunction of electrical equipment [5−7]. In particular, high-power IPT systems such as quick battery chargers for EVs generate higher level of EMF. Therefore, it is necessary to reduce EMI noise to widespread use of the IPT system.

In order to reduce EMF, many studies have been conducted on circuit topologies, modulation methods and configurations of transmission coils [5−13]. In particular, non-resonant reactive shield and active shield, which are focused on the configurations of the transmission coils, have been proposed [11−13].

Non-resonant reactive shielding methods require additional short-circuited coils in order to reduce EMF [11]. The magnetic flux induces a current which cancels the leakage magnetic field in the short-circuited coils when a leakage magnetic flux crosses the short-circuited coils. However, the EMF-reduction effectiveness is low at the place far from the canceling coils because the magnetomotive force of the canceling coil is limited by the interlinkage magnetic flux [11].

On the other hand, the active shielding method employs canceling coils which are connected to the main transmission coils or additional power sources [11−13]. In this method, the current flowing in the canceling coils is controllable with the main coils or the power sources. Therefore, the cancellation of the magnetic field becomes more effective compared to the non-resonant reactive shielding method because the magnetic field generated by the canceling coils are controllable [11].

The reduction effect of EMF by adding coils has been reported in several papers [11−13]. Nevertheless, the influences on parameter variations of the transmission coil due to the additional coils have not been analytically discussed. In particular, the magnetic flux generated by the canceling coils not only reduces the EMF but also crosses the main coils as an interlinkage flux. Thus, the self-inductance and the mutual inductance of the entire transmission coil are changed due to the additional coils. This variation of the self-inductance changes the resonant frequency. Thus, the transmission power or the efficiency might be decreased compared that of the non-canceling coils. This problem in the past work is that the influences of attaching the canceling coils to the entire IPT systems are not discussed enough.

In this paper, the effect of the canceling coils is revealed as focusing on the variations of the equivalent self-inductance and the equivalent mutual inductance of the entire transmission coil, which is theoretically analyzed using a model of a four-winding transformer. The new contribution of this paper is providing a general analytical model and design criteria in order to reduce the parameter verification for the EMF canceling coils. In particular, the canceling coils are connected in parallel to the main transmission coils when the non-resonant reactive shielding method or the active shielding method are introduced in order to reduce EMF of transmission coils system. The equivalent self-inductances and the equivalent coupling coefficient taking into account the influence of the canceling coils are calculated from a view of the entire transmission system. Then, the calculation results are confirmed with measurement of the equivalent self-inductances and the equivalent coupling coefficient in

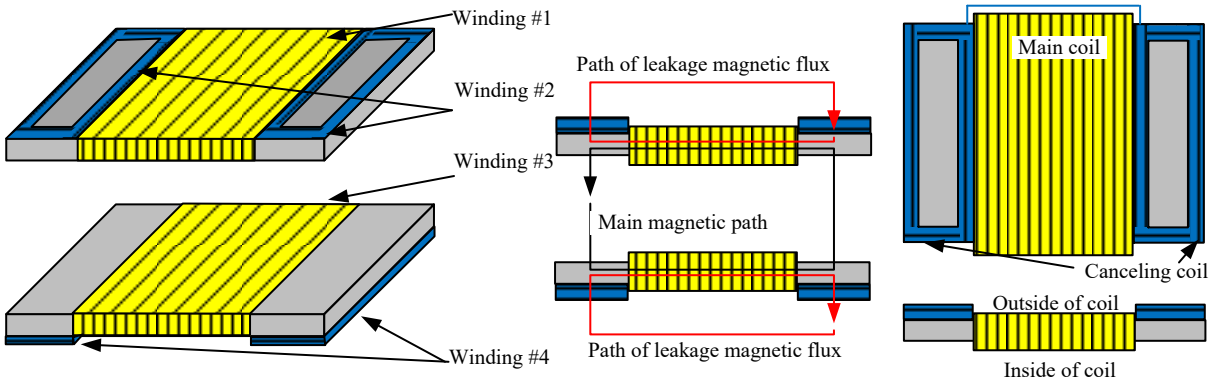

(a) Outline of transmission coil. (b) Front view with magnetic paths. (c) Configuration of coil at one side.

Fig. 1. Investigated model of transmission coil as example. The solenoid-type transmission coil with the canceling coils (winding #2 and winding #4). EMF upper and under cores is reduced by the canceling coils.

prototypes of the four-winding transformer. Moreover, the effect of EMF reduction is simulated when the prototypes are installed to the 1-kW IPT systems.

II. Configuration of Transmission Coils

In this section, the equivalent self-inductance and the equivalent coupling coefficient are formulated by a model of the multi-winding transformer when the canceling coils are connected to the main coils in parallel or short-circuited. The equivalent self-inductance is defined as self-inductances from a view of a primary side or secondary side of the entire transmission coil. The equivalent coupling coefficient is defined as a coupling coefficient between the primary side and the secondary side. Both of the equivalent values are essential to design a resonant frequency and a transmission power for IPT systems.

A. Analytical Model with Four-winding Transformer

Figure 1 shows the schematic of the analyzed transmission coils. Although following analysis is possible to be applied to general transmission coils, which fulfill some conditions as mentioned later, the solenoid-type transmission coil is analyzed as an example. The transmission coil behaves as the four-winding transformer. In order to avoid the additional core, the canceling coil is wired on the same core of the main coil. The main coils, e.g., winding #1 and winding #3, are wired on the cores to the form of the solenoid coils, whereas the canceling coils, e.g., winding #2 and winding #4, form a pair of the serial rectangular coil. As shown in Fig. 1(a), the canceling coils are placed on the outside of the primary and secondary cores in order to reduce EMF which emits in the direction of the upper and below the transmission coils.

Due to the placement of the canceling coils, the mutual inductances between following windings, e.g., winding #2 and winding #3, winding #2 and winding #4, and winding #4 and winding #1, are negligibly weak. Thus, the relationship between current and voltage of each coil in Fig. 1 is expressed by the four-order inductance matrix as

$$\begin{pmatrix} v_1 \\ v_2 \\ v_3 \\ v_4 \end{pmatrix} = \begin{pmatrix} L_{11} & L_{12} & L_{13} & 0 \\ L_{12} & L_{22} & 0 & 0 \\ L_{13} & 0 & L_{11} & L_{12} \\ 0 & 0 & L_{12} & L_{22} \end{pmatrix} \frac{d}{dt} \begin{pmatrix} i_1 \\ i_2 \\ i_3 \\ i_4 \end{pmatrix}$$

$$= L \begin{pmatrix} 1 & k_c\sqrt{\alpha} & k_M & 0 \\ k_c\sqrt{\alpha} & \alpha & 0 & 0 \\ k_M & 0 & 1 & k_c\sqrt{\alpha} \\ 0 & 0 & k_c\sqrt{\alpha} & \alpha \end{pmatrix} \frac{d}{dt} \begin{pmatrix} i_1 \\ i_2 \\ i_3 \\ i_4 \end{pmatrix} \quad (1),$$

where v_m and i_m (m = 1, 2, 3, and 4) are the input voltage and the current of the winding m , L_{mm} is the self-inductance of the winding m, and L_{mn} ($m \neq n$, n = 1, 2, 3, or 4) is the mutual inductance between the winding m and the winding n, respectively. Here, L is equal to L_{11}. Note that k_M and k_c are the coupling coefficients between the main-coil to the main-coil or the canceling-coil, respectively. Moreover, α is the inductance ratio L_{13} / L.

Figure 2 shows the connection diagrams of the non-resonant reactive shielding method and the active shielding method. In the active shielding method, both of the cases, where the canceling coils are connected as the common-mode coils and the differential-mode coils, are considered. In particular, the common mode coils result in the positive mutual inductance between the parallel-connected coils, whereas the negative mutual inductance between the parallel-connected coils occurs in the differential mode coils.

III. Calculation of Equivalent Parameters

A. Inverse Matrix of Inductance Matrix

In order to clarify the equivalent self-inductance and the equivalent coupling coefficients, the inductance matrix is calculated. It is convenient to calculate the current of the coils from the input voltage with the inverse matrix of the inductance matrix when conditions of the input voltage is decided as shown in Fig. 2. The relationship between current and voltage of each coil in Fig. 1 is also expressed by a four-order inverse matrix in (2) (bottom of next page) and (3)

$$\det L = \alpha L\left\{\left(1+k_c\right)^2\left(1-k_c\right)^2 - {k_M}^2\right\} \quad \text{..... (3).}$$

where det$L$ is the determinant of the four-order inductance matrix in (1).

B. Short-circuited Coil

When the canceling coils are shorted as shown in Fig. 2(a), the input voltage is $v_1 = v_p$, $v_3 = v_s$ and $v_2 = v_4 = 0$. Hence, the input current is expressed by

$$\begin{pmatrix} i_1 \\ i_2 \\ i_3 \\ i_4 \end{pmatrix} = \frac{1}{\det L} \begin{pmatrix} \alpha\left(1-k_c^{\,2}\right)\int v_p dt - \alpha k_M \int v_s dt \\ -\sqrt{\alpha}k_c\left(1-k_c^{\,2}\right)\int v_p dt + \sqrt{\alpha}k_c k_M \int v_s dt \\ -\alpha k_M \int v_p dt + \alpha\left(1-k_c^{\,2}\right)\int v_s dt \\ \sqrt{\alpha}k_c k_M \int v_p dt - \sqrt{\alpha}k_c\left(1-k_c^{\,2}\right)\int v_s dt \end{pmatrix} \quad \cdots\cdots (4).$$

In addition, the conditions of the input current $i_1 = i_p$, $i_3 = i_s$ are considered. The relationship between the voltage and the current of the entire transmission coils is shown as

$$\begin{pmatrix} i_p \\ i_s \end{pmatrix} = \begin{pmatrix} i_1 \\ i_3 \end{pmatrix} = \frac{\alpha}{\det L} \begin{pmatrix} 1-k_c^{\,2} & -k_M \\ -k_M & 1-k_c^{\,2} \end{pmatrix} \begin{pmatrix} \int v_p dt \\ \int v_s dt \end{pmatrix} \quad \cdots\cdots (5),$$

$$\begin{pmatrix} v_p \\ v_s \end{pmatrix} = \begin{pmatrix} L_{peq\_short} & M_{eq\_short} \\ M_{eq\_short} & L_{seq\_short} \end{pmatrix} \frac{d}{dt} \begin{pmatrix} i_p \\ i_s \end{pmatrix} = L \begin{pmatrix} 1-k_c^{\,2} & k_M \\ k_M & 1-k_c^{\,2} \end{pmatrix} \frac{d}{dt} \begin{pmatrix} i_p \\ i_s \end{pmatrix} \quad \cdots\cdots (6),$$

where L_{peq_short} is the equivalent self-inductance of the primary side, L_{seq_short} is the equivalent self-inductance of the secondary side, and M_{eq_short} is the equivalent mutual inductances between the primary side and the secondary side.

Through the calculation, the self-inductance and the coupling coefficient of the entire transmission coil are changed from the original values L and k_M, respectively. The equivalent self-inductance $L_{eq\text{-}short}$ ($= L_{peq\_short} = L_{seq\_short}$) and the equivalent coupling coefficient k_{eq_short} are expressed in (7) and (8).

$$L_{eq\_short} = L\left(1-k_c^{\,2}\right) \quad \cdots\cdots (7)$$

$$k_{eq\_short} = \frac{M_{eq\_short}}{L_{eq\_short}} = \frac{k_M}{1-k_c^{\,2}} \quad \cdots\cdots (8)$$

C. Commom-mode Coil

The conditions of the input voltage is $v_1 = v_2 = v_p$ and $v_3 = v_4 = v_s$. Hence, when the canceling coils are connected to the main coils as the common-mode coils as shown in Fig. 2 (b), the input current is expressed by (9).

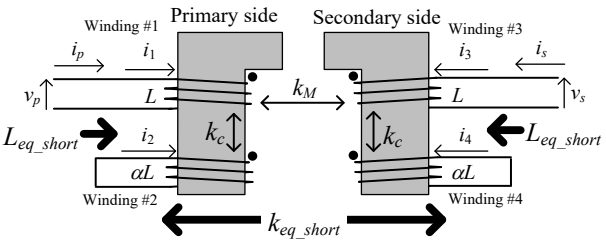

(a) Short-circuited canceling coils.

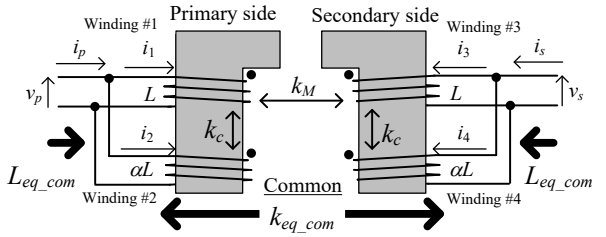

(b) Canceling coils connected as common-mode coils.

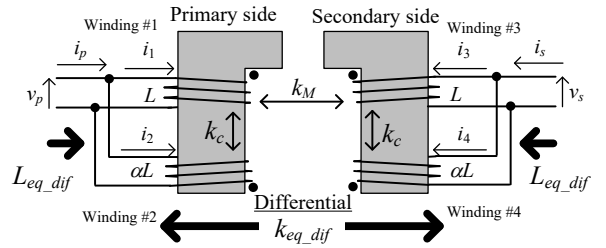

(c) Canceling coils connected as differential-mode coils.

Fig. 2. Connection diagrams of main coils and canceling coils.

In addition, the conditions of the input current $i_p = i_1 + i_2$, $i_s = i_3 + i_4$ are considered. The relationship between the voltage and the current of the entire transmission coils is shown in (10) and (11) (next page), where L_{peq_com} is the equivalent self-inductance of the primary side, L_{seq_com} is the equivalent self-inductance of the secondary side, and M_{eq_com} is the equivalent mutual inductances between the primary side and the secondary side. The equivalent self-inductance L_{eq_com} ($= L_{peq\_com} = L_{seq\_com}$) and the equivalent

---

$$\begin{pmatrix} i_1 \\ i_2 \\ i_3 \\ i_4 \end{pmatrix} = \begin{pmatrix} L_{11} & L_{12} & L_{13} & 0 \\ L_{12} & L_{22} & 0 & 0 \\ L_{13} & 0 & L_{11} & L_{12} \\ 0 & 0 & L_{12} & L_{22} \end{pmatrix}^{-1} \begin{pmatrix} \int v_1 dt \\ \int v_2 dt \\ \int v_3 dt \\ \int v_4 dt \end{pmatrix} = \frac{1}{\det L} \begin{pmatrix} \alpha\left(1-k_c^{\,2}\right) & -\sqrt{\alpha}k_c\left(1-k_c^{\,2}\right) & -\alpha k_M & \sqrt{\alpha}k_c k_M \\ -\sqrt{\alpha}k_c\left(1-k_c^{\,2}\right) & \left(1-k_c^{\,2}\right)-k_M^{\,2} & \sqrt{\alpha}k_c k_M & -k_c^{\,2}k_M \\ -\alpha k_M & \sqrt{\alpha}k_c k_M & \alpha\left(1-k_c^{\,2}\right) & -\sqrt{\alpha}k_c\left(1-k_c^{\,2}\right) \\ \sqrt{\alpha}k_c k_M & -k_c^{\,2}k_M & -\sqrt{\alpha}k_c\left(1-k_c^{\,2}\right) & \left(1-k_c^{\,2}\right)-k_M^{\,2} \end{pmatrix} \begin{pmatrix} \int v_1 dt \\ \int v_2 dt \\ \int v_3 dt \\ \int v_4 dt \end{pmatrix} \quad (2)$$

$$\begin{pmatrix} i_1 \\ i_2 \\ i_3 \\ i_4 \end{pmatrix} = \frac{1}{\det L} \begin{pmatrix} \sqrt{\alpha}\left(\sqrt{\alpha}-k_c\right)\left(1-k_c^{\,2}\right)\int v_p dt - \sqrt{\alpha}\left(\sqrt{\alpha}-k_c\right)k_M \int v_s dt \\ \left\{\left(1-\sqrt{\alpha}k_c\right)\left(1-k_c^{\,2}\right)-k_M^{\,2}\right\}\int v_p dt + \left(\sqrt{\alpha}-k_c\right)k_c k_M \int v_s dt \\ -\sqrt{\alpha}\left(\sqrt{\alpha}-k_c\right)k_M \int v_p dt + \sqrt{\alpha}\left(\sqrt{\alpha}-k_c\right)\left(1-k_c^{\,2}\right)\int v_s dt \\ \left(\sqrt{\alpha}-k_c\right)k_c k_M \int v_p dt + \left\{\left(1-\sqrt{\alpha}k_c\right)\left(1-k_c^{\,2}\right)-k_M^{\,2}\right\}\int v_s dt \end{pmatrix} \quad (9)$$

coupling coefficient k_{eq_com} are expressed in (12) and (13).

$$L_{eq\_com} = \frac{\alpha L\left\{\left(1-k_c{}^2\right)\left(1+\alpha-2k_c\sqrt{\alpha}\right)-k_M{}^2\right\}}{\left(\alpha-2\sqrt{\alpha}k_c+1\right)^2-k_M{}^2} \quad \text{....(12)}$$

$$k_{eq\_com} = \frac{M_{eq\_com}}{L_{eq\_com}} = \frac{k_M\left(\sqrt{\alpha}-k_c\right)^2}{\left(1-k_c{}^2\right)\left(1+\alpha-2k_c\sqrt{\alpha}\right)-k_M{}^2} \quad \text{.....(13)}$$

D. Differential-mode Coil

The conditions of the input voltage is $v_1 = -v_2 = v_p$ and $v_3 = -v_4 = v_s$ when the canceling coils are connected to the main coils as the differential-mode coils as shown in Fig. 2 (c). Hence, the input current is expressed by (14).

In addition, the conditions on the input current $i_p = i_1 - i_2$, $i_s = i_3 - i_4$ are considered. The relationship between the voltage and the current of the entire transmission coils is shown in (15) and (16), where L_{peq_dif} is the equivalent self-inductance of the primary side, L_{seq_dif} is the equivalent self-inductance of the secondary side, and M_{eq_dif} is the equivalent mutual inductances between the primary side and the secondary side. The equivalent self-inductance L_{eq_dif} ($= L_{peq\_dif} = L_{seq\_dif}$) and the equivalent coupling coefficient k_{eq_dif} are expressed in (17) and (18).

$$L_{eq\_dif} = \frac{\alpha L\left\{\left(1-k_c{}^2\right)\left(1+\alpha+2k_c\sqrt{\alpha}\right)-k_M{}^2\right\}}{\left(\alpha+2\sqrt{\alpha}k_c+1\right)^2-k_M{}^2} \quad \text{....(17)}$$

$$k_{eq\_dif} = \frac{k_M\left(\sqrt{\alpha}+k_c\right)^2}{\left(1-k_c{}^2\right)\left(1+\alpha+2k_c\sqrt{\alpha}\right)-k_M{}^2} \quad \text{.....(18)}$$

E. Design Criteria of Canceling Coils

Figures 3 and 4 show the contour diagrams of the equivalent coupling coefficients and the equivalent self-inductances derived from Eqs. (7–8, 12–13, 17–18), respectively. It is noted that the coupling coefficient k_M is fixed at 0.2, whereas the coupling coefficient k_c and the self-inductance ratio α are variables. In particular, k_c is adjusted by changing installation location and configuration of the canceling coils, whereas α is also adjusted by changing the number of the turns of the canceling coils.

Figure 3(a) shows that k_{eq_short} is improved by increasing k_c, whereas k_{eq_short} is not varied by α. Meanwhile, Fig. 4(a) shows that the L_{eq_short} is decreased by increase k_c, and L_{eq_short} is not also varied by α. Hence, the parameter variation with the short-circuited canceling coils is not influenced by the number of the turns of the canceling coils.

$$\begin{pmatrix} i_p \\ i_s \end{pmatrix} = \begin{pmatrix} i_1+i_2 \\ i_3+i_4 \end{pmatrix} = \frac{1}{\det L}\begin{pmatrix} \left(\alpha-2\sqrt{\alpha}k_c+1\right)\left(1-k_c{}^2\right)-k_M{}^2 & -\left(\sqrt{\alpha}-k_c\right)^2 k_M \\ -\left(\sqrt{\alpha}-k_c\right)^2 k_M & \left(\alpha-2\sqrt{\alpha}k_c+1\right)\left(1-k_c{}^2\right)-k_M{}^2 \end{pmatrix}\begin{pmatrix} \int v_p dt \\ \int v_s dt \end{pmatrix} \quad (10)$$

$$\begin{pmatrix} v_p \\ v_s \end{pmatrix} = \begin{pmatrix} L_{peq\_com} & M_{eq\_com} \\ M_{eq\_com} & L_{seq\_com} \end{pmatrix}\frac{d}{dt}\begin{pmatrix} i_p \\ i_s \end{pmatrix}$$

$$= \frac{\alpha L}{\left(\alpha-2\sqrt{\alpha}k_c+1\right)^2-k_M{}^2}\begin{pmatrix} \left(\alpha-2\sqrt{\alpha}k_c+1\right)\left(1-k_c{}^2\right)-k_M{}^2 & \left(\sqrt{\alpha}-k_c\right)^2 k_M \\ \left(\sqrt{\alpha}-k_c\right)^2 k_M & \left(\alpha-2\sqrt{\alpha}k_c+1\right)\left(1-k_c{}^2\right)-k_M{}^2 \end{pmatrix}\frac{d}{dt}\begin{pmatrix} i_p \\ i_s \end{pmatrix} \quad (11)$$

$$\begin{pmatrix} i_1 \\ i_2 \\ i_3 \\ i_4 \end{pmatrix} = \frac{1}{\det L}\begin{pmatrix} \sqrt{\alpha}\left(\sqrt{\alpha}+k_c\right)\left(1-k_c{}^2\right)\int v_p dt - \sqrt{\alpha}\left(\sqrt{\alpha}+k_c\right)k_M\int v_s dt \\ \left\{-\left(1+\sqrt{\alpha}k_c\right)\left(1-k_c{}^2\right)+k_M{}^2\right\}\int v_p dt + \left(\sqrt{\alpha}+k_c\right)k_c k_M\int v_s dt \\ -\sqrt{\alpha}\left(\sqrt{\alpha}+k_c\right)k_M\int v_p dt + \sqrt{\alpha}\left(\sqrt{\alpha}+k_c\right)\left(1-k_c{}^2\right)\int v_s dt \\ \left(\sqrt{\alpha}+k_c\right)k_c k_M\int v_p dt + \left\{-\left(1+\sqrt{\alpha}k_c\right)\left(1-k_c{}^2\right)+k_M{}^2\right\}\int v_s dt \end{pmatrix} \quad (14)$$

$$\begin{pmatrix} i_p \\ i_s \end{pmatrix} = \begin{pmatrix} i_1-i_2 \\ i_3-i_4 \end{pmatrix} = \frac{1}{\det L}\begin{pmatrix} \left(\alpha+2\sqrt{\alpha}k_c+1\right)\left(1-k_c{}^2\right)-k_M{}^2 & -\left(\sqrt{\alpha}+k_c\right)^2 k_M \\ -\left(\sqrt{\alpha}+k_c\right)^2 k_M & \left(\alpha+2\sqrt{\alpha}k_c+1\right)\left(1-k_c{}^2\right)-k_M{}^2 \end{pmatrix}\begin{pmatrix} \int v_p dt \\ \int v_s dt \end{pmatrix} \quad (15)$$

$$\begin{pmatrix} v_p \\ v_s \end{pmatrix} = \begin{pmatrix} L_{peq\_dif} & M_{eq\_dif} \\ M_{eq\_dif} & L_{seq\_dif} \end{pmatrix}\frac{d}{dt}\begin{pmatrix} i_p \\ i_s \end{pmatrix}$$

$$= \frac{\alpha L}{\left(\alpha+2\sqrt{\alpha}k_c+1\right)^2-k_M{}^2}\begin{pmatrix} \left(\alpha+2\sqrt{\alpha}k_c+1\right)\left(1-k_c{}^2\right)-k_M{}^2 & \left(\sqrt{\alpha}+k_c\right)^2 k_M \\ \left(\sqrt{\alpha}+k_c\right)^2 k_M & \left(\alpha+2\sqrt{\alpha}k_c+1\right)\left(1-k_c{}^2\right)-k_M{}^2 \end{pmatrix}\frac{d}{dt}\begin{pmatrix} i_p \\ i_s \end{pmatrix} \quad (16)$$

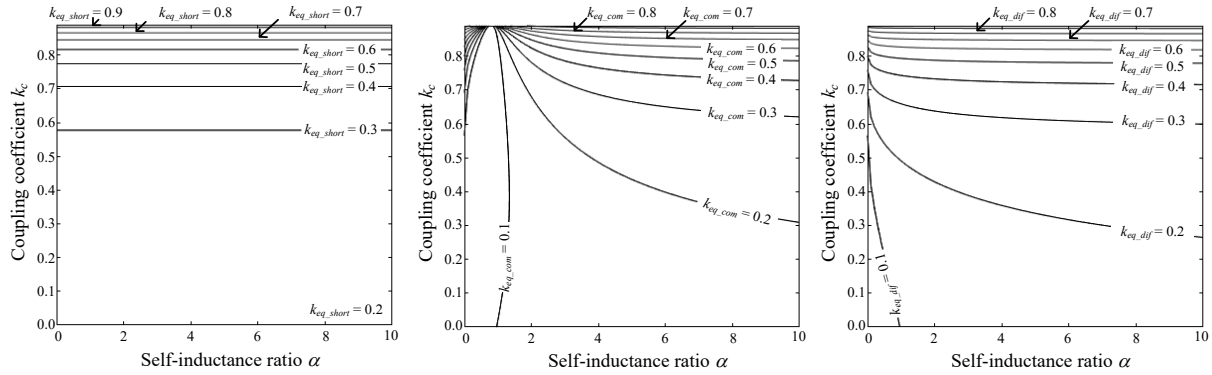

(a) Short-circuited. (b) Common mode. (c) Differential mode.

Fig. 3. Relationship among equivalent coupling coefficients, coupling coefficient between main coil and canceling coil, and self-inductance ratio. The coupling coefficient k_M is 0.2. Variation range of the coupling coefficient between the main coil and the canceling coil k_c is from 0 to 0.89, whereas range of the self-inductance ratio α is from 0 to 10.

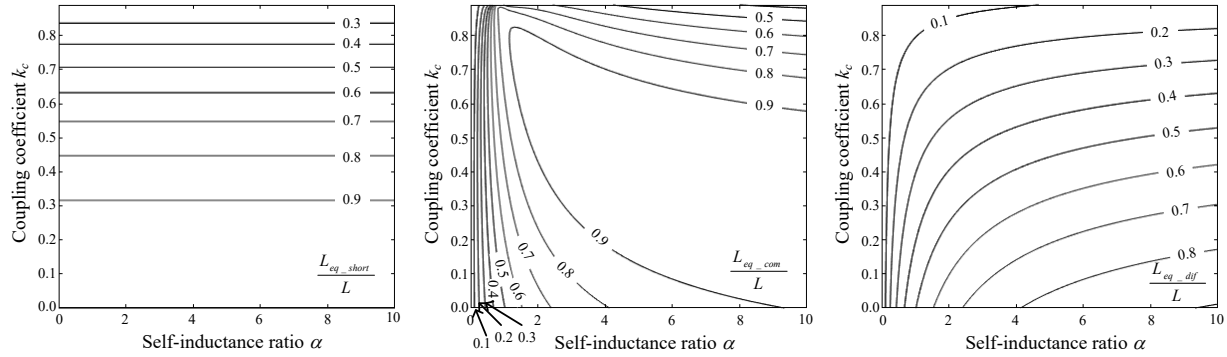

(a) Short-circuited. (b) Common mode. (c) Differential mode.

Fig. 4. Relationship among ratio of equivalent self-inductances to self-inductance of main windings, coupling coefficient between main coils and canceling coils, and self-inductance ratio. Conditions of k_M, k_c, and α are same as in Fig. 3.

Figure 3(b) shows that k_{eq_com} is improved by increasing k_c or α. Figure 4(b) shows that L_{eq_com} is decreasing due to the increase in k_c or the decrease in α. Thus, in order to avoid the parameter variation which is caused by the common-mode-connected canceling coils, not only the number of the turns of the canceling coils should be designed larger than the number of the turns of the main coils, but also the canceling coils have to be placed close to the main coils.

Figure 3(c) shows that k_{eq_dif} is improved in the range of high k_c and high α. Meanwhile, Fig. 4(c) shows that L_{eq_dif} is decreasing due to the high k_c and the decrease in α. Therefore, not only the winding turn should be much larger than the main coils, but also the canceling coils have to be installed apart from the main coil in order to avoid the parameter variation which is caused by the differential-mode-connected canceling coils.

However, setting the canceling coils apart from the main coils degrades a canceling performance of EMF. There is the trade-off between the parameter variation (decreasing of the equivalent self-inductance) and the canceling performance. Thus, an operation frequency or the construction of a transmission coil should be redesigned, when the canceling coils are installed in order to reduce EMF.

As a conclusion, it is shown that the design criteria for the three connection methods of the canceling coils at the view point of avoiding the parameter variations as follows:

1) the short-circuited connection (non-resonant reactive shield)
- the long distance between the main coils and the canceling coils.
- the low self-inductance of the canceling coils.

2) the common-mode connection
- installation of the canceling coils by the main coils.
- twice times or more the number of the turn of the canceling coils compared with the main coils.

3) the differential-mode connection
- the long distance between the main coils and the canceling coils.
- twice or more the number of the turn of the canceling coils compared with the main coils.

The advantage of avoiding the parameter variations is reducing the mismatch between the operation frequency and the resonant frequency, which is necessary to operate IPT systems under the conditions of the high efficiency and the high power transmission.

IV. Experimental Verification with Prototype Transmission Coil

The self-inductances and the mutual inductances of the wired coils are measured in order to confirm Eqs. (7–8, 12–13, 17–18) with the prototype four-winding transmission coil.

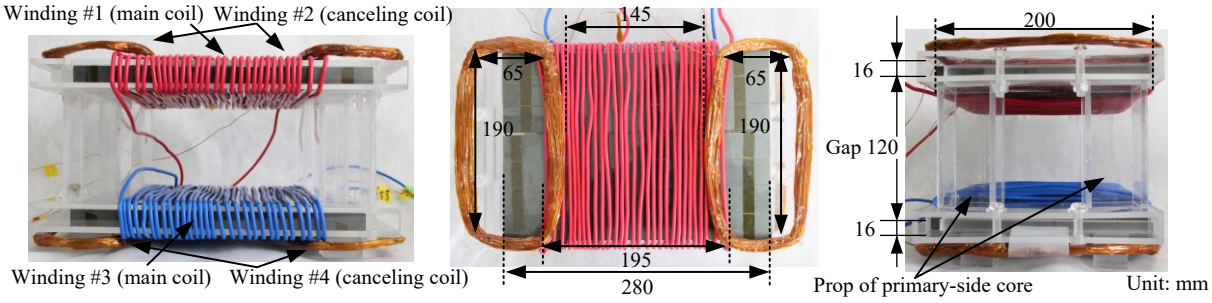

(a) Front view. (b) Top view. (c) Side view.

Fig. 5. Outline of prototype four-winding transmission coils. The main coils are wired on center of the cores (winding #1 and winding #3). The canceling coils are put on top of the primary core and bottom of the secondary core (winding #2 and winding #4). The canceling coils construct the serial two coils. The four props support the primary-side core.

Table I. Experimental results: equivalent coupling coefficient and inductances of prototype four-winding transformer.

Connection of canceling coils		Short-circuited	Common mode	Differential mode
Inductance matrix as 4-winding transformer		$\begin{pmatrix} 399 & 432 & 70.4 & 12.2 \\ 432 & 3120 & 12.8 & 6.7 \\ 70.5 & 12.8 & 393 & 422 \\ 12.2 & 6.7 & 422 & 3010 \end{pmatrix}$ [μH]		
Self-inductance of main winding L	Measured value	396 μH		
Self-inductance ratio α	Measured value	7.94		
Coupling coefficient k_c	Measured value	0.382		
Coupling coefficient k_M	Measured value	0.178		
Equivalent primary self-inductance	Measured value	334 μH	396 μH	236 μH
	Calculated value	338 μH	394 μH	241 μH
Error of calculated equivalent primary self-inductance		1.3%	0.6%	2.3%
Equivalent secondary self-inductance	Measured value	332 μH	391 μH	235 μH
	Calculated value	338 μH	394 μH	241 μH
Error of calculated equivalent secondary self-inductance		1.9%	0.7%	2.7%
Equivalent mutual inductance	Measured value	67.5 μH	73.0 μH	43.3 μH
	Calculated value	70.4 μH	72.1 μH	46.6 μH
Equivalent coupling coefficient	Measured value	0.203	0.185	0.184
	Calculated value	0.208	0.183	0.193
Error of calculated coupling coefficient		2.7%	1.2%	4.9%

Figure 5 shows the prototype of the transmission coil. In order to shield EMF on the top and below, the canceling coils shaped double-D are put on the outside cores. The core material is ferrite (TDK Corp., N87). The number of turns of the main coils is 30 with 3.5-mm^2 insulated wires, whereas the number of turn of the canceling coils is 130 with enameled wires. Note that the number of turns of the primary side and the secondary side are the same.

Table I shows the measurement results of the four-order inductance matrix, the equivalent self-inductances and the equivalent coupling coefficients in the each connection. In order to compare the equivalent self-inductance, the equivalent mutual inductance, and the equivalent coupling coefficient, both the measured values and the calculated values are shown.

In particular, the calculated values of the equivalent self-inductances correspond to the measured values with a maximum error of 2.7%. The self-inductance is the important factor because the IPT system should be designed to resonate at the transmission frequency. Thus, a precise calculation is crucial for the design of the IPT system. Besides, the maximum error of the equivalent coupling coefficients is 4.9%, which is larger than the error of the equivalent self-inductance because of the influence of the ignored magnetic coupling between following windings, i.e., winding #2 to winding #3, winding #2 to winding #4, and winding #4 to winding #1.

V. EMF Reduction with Canceling Coils

A. Circuit and Model Configuration

In order to confirm the effect of the EMF reduction, the prototype transmission coil is simulated with JMAG (JSOL Corporation). JMAG is a software for the electromagnetic field analysis with a finite element method.

Figure 6 shows the circuit configuration in the simulation model, whereas Table II shows the specification of the circuit. The IPT system is constructed with S/S topology, which has the resonant capacitors connected to both of the primary side and secondary side of the transmission coil in series. The input voltage is the sinusoidal wave for focusing on fundamental frequency. The capacitances of the resonant capacitors C_{s1}, C_{s2} are decided in order to resonate with the considered L at a resonance frequency of 84.75 kHz. Noted that operating frequency is decided by the resonant conditions of the resonance capacitances and the equivalent self-inductance such as L_{eq_short}, L_{eq_com}, or L_{eq_dif}. The output power is 1 kW by adjusting the value of the equivalent load resistance

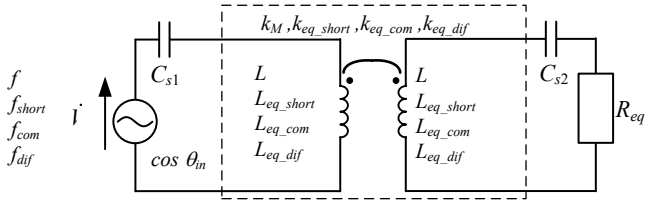

Equivalent circuit of prototype four-winding transmission coil

Fig. 6. Circuit configuration of simulation model. The prototype four-winding transformer is equivalent to the two-winding transformer when the canceling coils are shorted or connected to the main coils in parallel. For individual connection such as when the canceling coils are shorted, the equivalent self-inductance, the equivalent coupling coefficient and the operation frequency are chosen L_{eq_short}, k_{eq_short} and f_{short} differently.

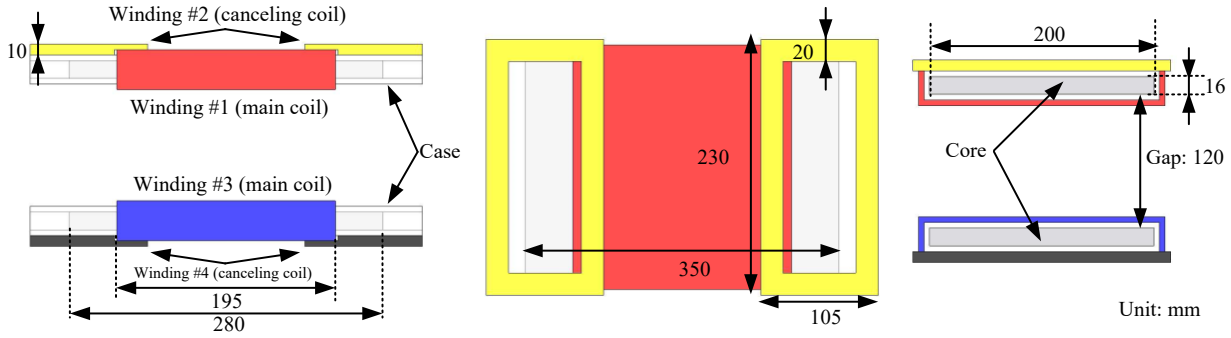

(a) Front view. (b) Top view. (c) Side view.

Fig. 7. Outline of CAD model of prototype four-winding transmission coil. The size of the cores and the cases matches the prototype four-winding transformer; the coils are constructed as the solid model, and the material of the cores is PC40. The cases are treated as air, whereas the thickness of the cases and the main coils is 5 mm.

Table II. Simulation conditions.

Parameter	Symbol	Value
Input AC voltage	V_{in}	252 Vrms
Rated power	P	1.0 kW
Operation frequency without canceling coils	f	84.75 kHz
Operation frequency of short-circuited operation	f_{short}	95.00 kHz
Operation frequency of common-mode operation	f_{com}	85.40 kHz
Operation frequency of differential-mode operation	f_{dif}	115.5 kHz
Resonant capacitors	C_{s1} ,C_{s2}	8.56 nF

R_{eq} because the output current of the S/S resonant circuit is inversely proportional to the equivalent mutual inductance of the transmission coil at the LC resonance.

Figure 7 shows the computer-aided-design (CAD) model of the transmission coil on JMAG. The structure and the size of the CAD model are based on the prtototype four-winding transmission coil as shown in Fig. 5. The wires are expressed as the colored solid models. Noted that the eddy current and hysteresis loss are not considered.

B. EMF Reduction Effect with Canceling Coils

Figure 8 shows the simulation results of the magnetic flux distribution under the each condition. The result is obtained on the cross-section of the center of the transmission coil as a representative case. Note that the input power factor cos θ_{in} is unity when the operation frequencies of Fig. 8(a)–(d) are 84.75 kHz, 95.00 kHz, 85.40 kHz, 115.5 kHz, respectively.

The flux distributions on the top and bottom of the transmission coils decreases with the short-circuited connection and differential-mode connection in comparison with the flux distribution without the canceling coils. The magnetic flux distribution of Fig. 8(a)–(d) are 13.8 μT, 9.41 μT, 12.6 μT, and 8.06 μT at the 50-cm bottom of the secondary core as the representative values, respectively. In addition, the magnetic density at the outside of the canceling coil decreases by the canceling coils. Moreover, the effect of EMF reduction is more effective with the differential operation than that with the short-circuited connection.

VI. CONCLUSION

In this paper, the effect of the canceling coils on the parameter variation of the IPT system was considered regarding to the equivalent self-inductance and the equivalent coupling coefficient. Three connection methods of the canceling coils, i.e. the short-circuited connection, the common-mode connection and the differential-mode connection, were evaluated.

The calculated equivalent values agreed with the measured values through the inductance measurement using the prototype transmission coil attached the canceling coils. The relative error between the calculated values and measured values was 4.9%.

In addition, EMF reduction near the canceling coils were confirmed with the short-circuit connection (by 32%) and the differential-mode connection (by 41%) in the simulation using JMAG.

Above of the results, the design criteria focusing on avoiding the parameter verifications are as follows:

- the canceling coils far from the main coils at the short-circuited connection.
- the canceling coils closed to the main coils with

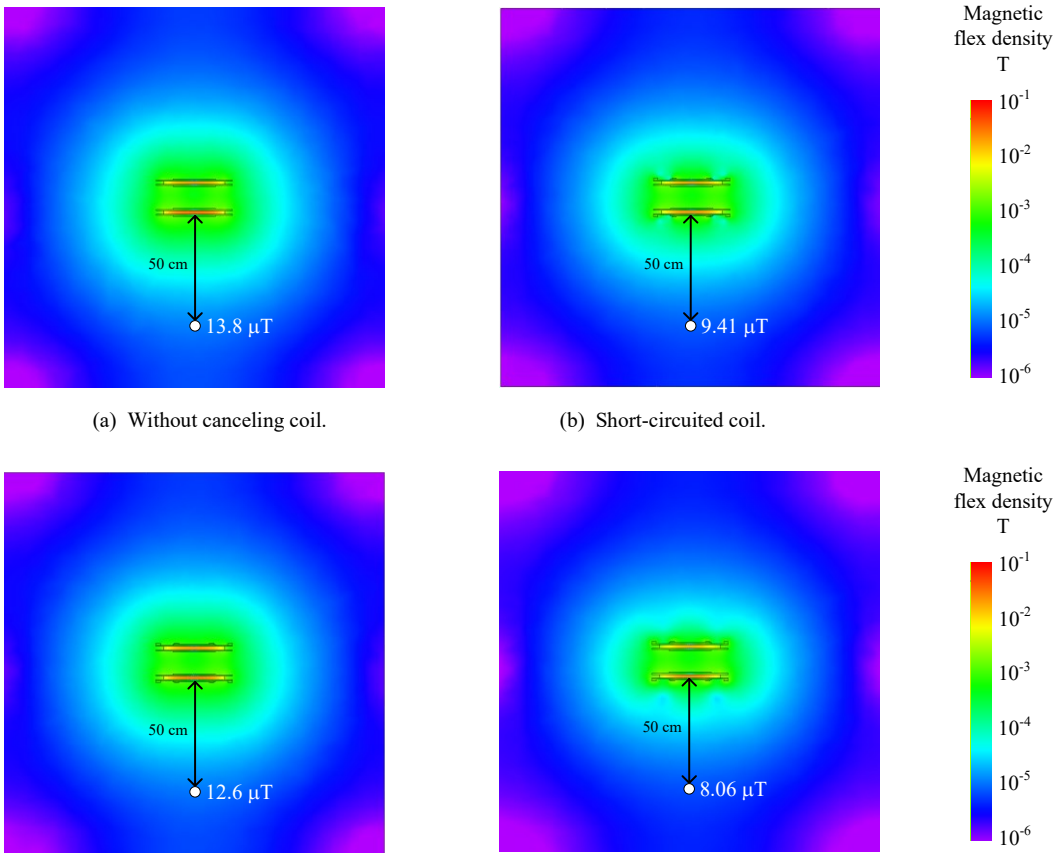

(a) Without canceling coil. (b) Short-circuited coil.

(c) Common-mode coil. (d) Differential-mode coil.

Fig. 8. Magnetic flux distribution of prototype transmission coil. The transmission coils are placed at the center of the contour plots (orange or yellow area). The upper-side core is the primary side. The bottom-side core is the secondary side. Note that the operation frequency is different for each the simulation conditions, which are shown in Table II. Transmission powers of without-canceling coil, short-circuited connection, common-mode connection and differential-mode connection are 991 W, 1.16 kW, 1.03 kW and 1.27 kW, respectively.

the large number of the turn at the common-mode connection.

- the canceling coils far from the main coils with the large number of the turn at the differential-mode connection.

Future plans are considerations of the parameter verifications introduced cross couplings between canceling coils.

REFERENCES

[1] T. Mizuno, T. Ueda, S. Yachi, R. Ohtomo and Y. Goto: "Dependence of Efficiency on Wire Type and Number of Strands of Litz Wire for Wireless Power Transfer of Magnetic Resonant Coupling", IEEJ Journal of Industry Applications, Vol. 3, No. 1, pp. 35-40 (2014)

[2] H. Ishida, H. Furukawa and T. Kyoden: "Development of Design Methodology for 60 Hz Wireless Power Transmission System", IEEJ Journal of Industry Applications, Vol. 5, No. 6, pp. 429-438 (2016)

[3] K. Kusaka, and J. Itoh: "Development Trends of Inductive Power Transfer Systems Utilizing Electromagnetic Induction with Focus on Transmission Frequency and Transmission Power", IEEJ Journal of Industry Applications, Vol. 137, No. 5, pp. 328-339 (2017)

[4] R. Ota, N. Hoshi and J. Haruna: "Design of Compensation Capacitor in S/P Topology of Inductive Power Transfer System with Buck or Boost Converter on Secondary Side", IEEJ Journal of Industry Applications, Vol. 4, No. 4, pp. 476-485 (2015)

[5] Su Y. Choi, Beom W. Gu, Seog Y. Jeong and Chun T. Rim: "Advances in Wireless Power Transfer Systems for Roadway-Powered Electric Vehicles", IEEE Trans. PE, Vol.3, No.1 pp.18 - 36 (2015)

[6] D. Shimode, T. Murai and S. Fujiwara: "A Study of Structure of Inductive Power Transfer Coil for Railway Vehicles", IEEJ Journal of Industry Applications, Vol. 4, No. 5, pp. 550-558 (2015)

[7] T. Watanabe and M. Ishida: "Study on the influence of the magnetic field and the induced electrical field in human bodies by wireless charging systems", EVTec and APE 2016, (2016)

[8] K. Kusaka, K. Inoue and J. Itoh: "Radiation Noise Reduction using Spread Spectrum for Inductive Power Transfer Systems considering Misalignment of Coils", Energy Conversion Congress and Exposition, pp. 5507-5514 (2017)

[9] T. Campi and Silvano Cruciani Mauro Feliziani: "Magnetic Shielding of Wireless Power Transfer Systems", Institute of Electronics, Information and Communication Engineers, 15A-H1, pp. 422-425 (2014)

[10] S. Kim, H. Park, J. Kim, J. Kim, and S. Ahn: "Design and Analysis of a Resonant Reactive Shield for a Wireless Power Electric Vehicle", IEEE TRANSACTIONS ON MICROWAVE THEORY AND TECHNIQUES, Vol. 62, No. 4, pp. 1057-1066 (2014)

[11] J. Park, D. Kim, K. Hwang, H. Ho Park and S. Il Kwak: "A Resonant Reactive Shielding for Planar Wireless Power Transfer System in Smartphone Application", IEEE TRANSACTIONS ON ELECTROMAGNETIC COMPATIBILITY, Vol. 59, No. 2, pp. 695-703 (2017)

[12] T. Shijo, K. Ogawa, M. Suzuki, Y. Kanekiyo and M. Ishida: "EMI Reduction Technology in 85 kHz Band 44 kW Wireless Power Transfer System for Rapid Contactless Charging of Electric Bus", IEEE Energy Conversion Congress and Exposition (2016)

[13] S. Lee et al., "Active EMF cancellation method for I-type pickup of online electric vehicles," in Proc. IEEE Appl. Power Electron. Conf. Expo., pp. 1980-1983 (2011)